Recent Results from CLEO II

JIM ALEXANDER

Department of Physics, Cornell University, Ithaca, New York 14953

ABSTRACT

Results are presented on $\Upsilon(4S) \to$ non-$B\bar{B}$ final states; D^* branching ratios; D^0 branching ratios to final states containing a π^0, η, or η'; and D_s branching ratios to final states containing the η or η'.

Presented at the SLAC Summer Institute on Particle Physics,
Stanford, California, August 5-16, 1991

1. Introduction

The CLEO experiment, operating at an e^+e^- center of mass energy of about 10GeV, is designed to explore many aspects of heavy quark physics. This note reports on results obtained with the upgraded CLEO II detector on decays of the $\Upsilon(4S)$ resonance and various charmed mesons.

Since the start of CLEO II operation in the fall of 1989, almost $1fb^{-1}$ of data has been collected, including $497pb^{-1}$ on the 4S resonance, 230 pb^{-1} at a center of mass energy 52 MeV below the 4S, 160 pb^{-1} at the $\Upsilon(3S)$, and $70pb^{-1}$ just above the 4S. During the winter and spring of 1991, the CESR storage ring achieved average luminosities of 30-40pb^{-1} per week.

2. The CLEO II Detector

The CLEO II detector, illustrated in figure 1, differs from CLEO I in many respects. It has new muon chambers, a new straw tube vertex detector, a new superconducting coil operating at 1.5T, new time of flight counters with 150ps resolution in the barrel, and an 7800 crystal CsI calorimeter. The calorimeter has brought new power to CLEO II in the clean detection of π^0s and ηs, permitting high statistics measurements of decay modes hitherto at the margin or just below the threshold of detection.

The performance of the calorimeter is illustrated in figures 2 — 4. Figure 2 shows the energy resolution of the calorimeter as measured with photons and electrons, and computed by Monte Carlo. The energy resolution may be characterized by $\sigma_E \approx 2.1\%/E^{1/4}$. Angular resolution, shown in figure 3 varies from about $3mrad$ at high momenta to $10mrad$ at low momenta. In the two-photon mass spectra shown in figure 4, one can see both a clear π^0 peak at all momenta, and an η peak at momenta above 1 GeV. The mass resolution of the π^0 peak varies from 4 to 7 MeV over the range of momenta shown.

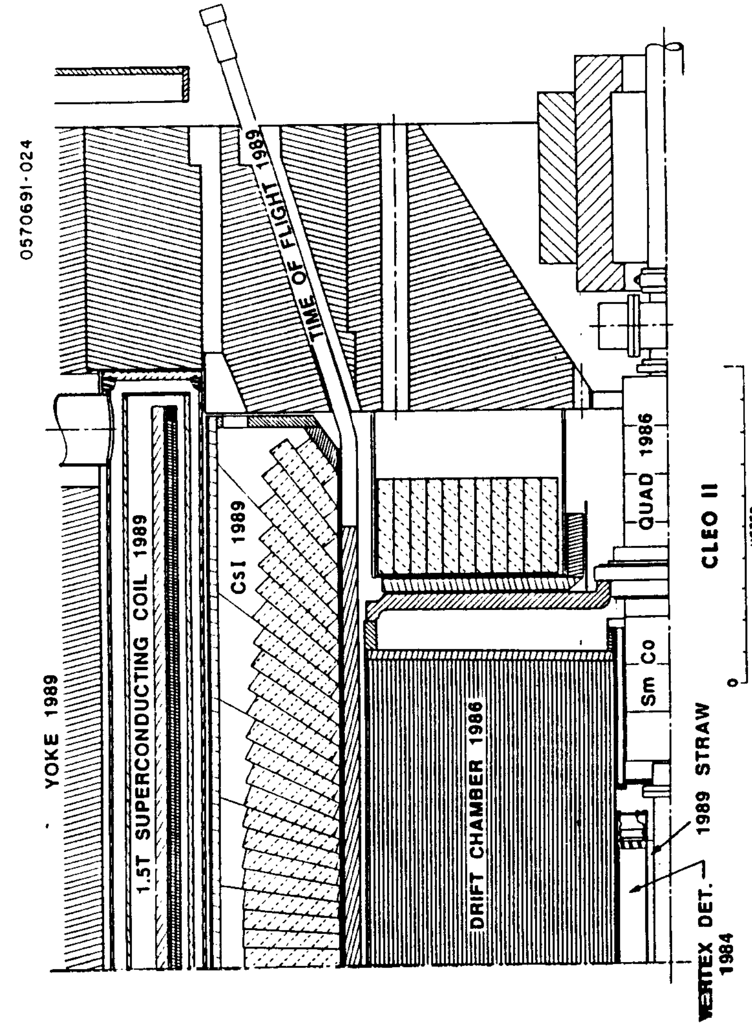

1. Quarter section of the CLEO II detector.

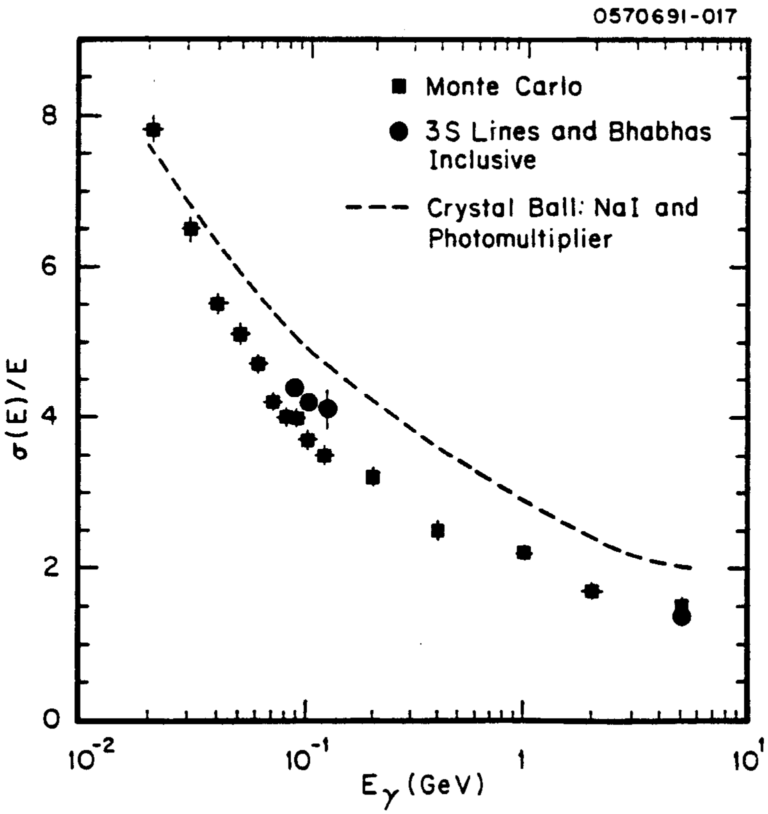

2. Energy resolution of the calorimeter.

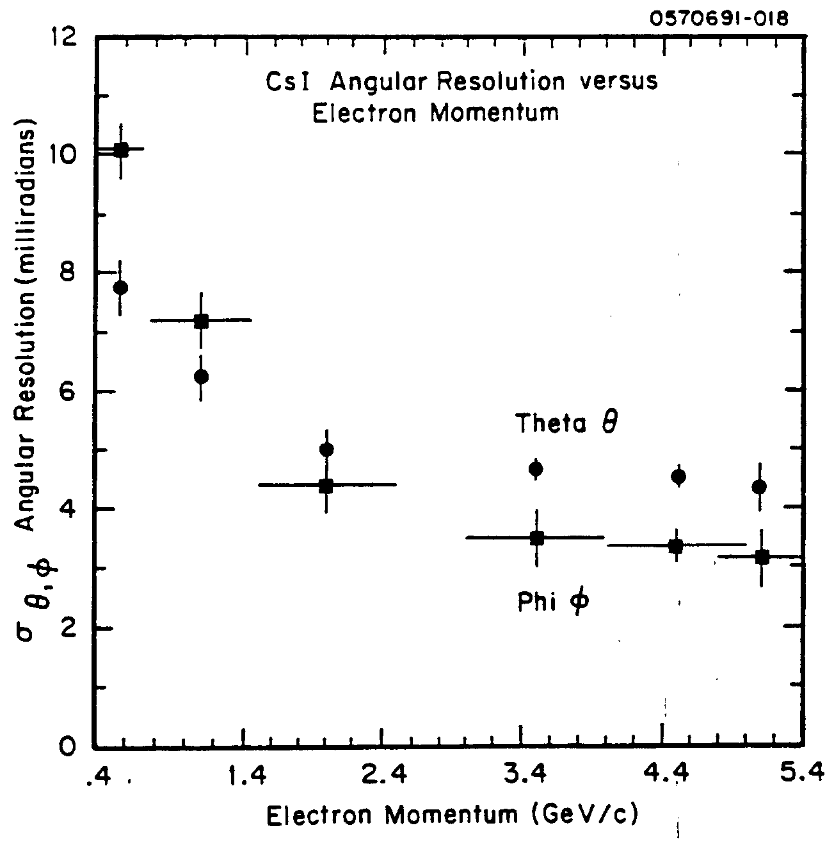

3. Angular resolution for electrons in the calorimeter.

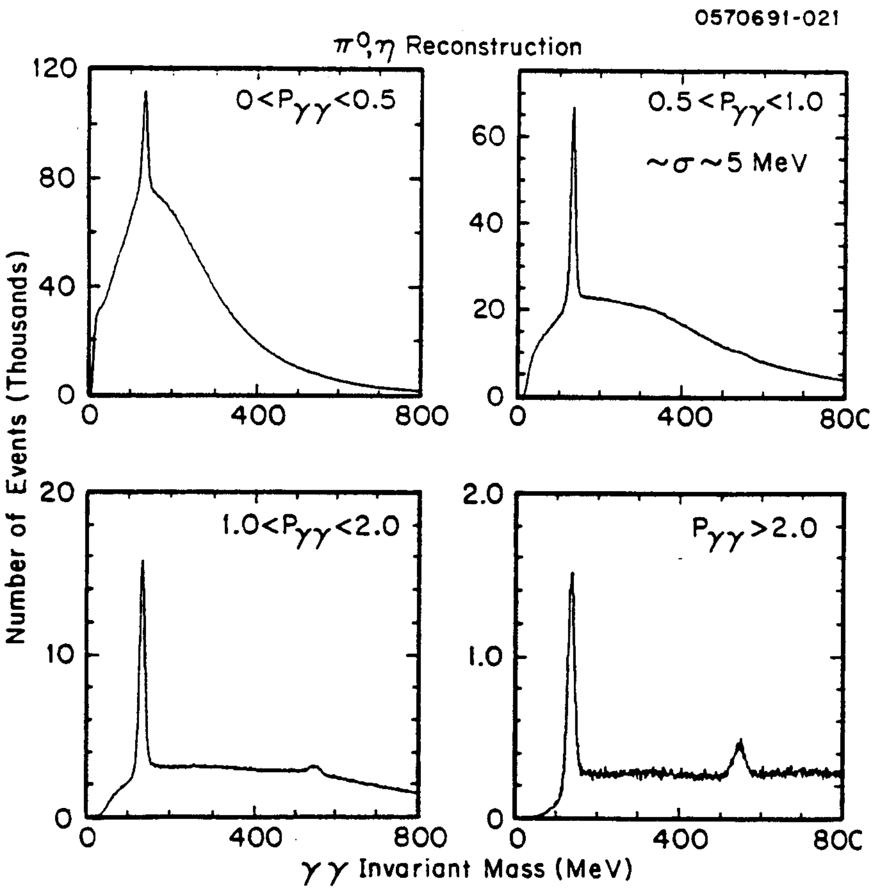

4. Two-photon invariant mass plots in 4 momentum ranges, as labelled. The π^0 peak is cleanly visible at all momenta. The η peak becomes prominent at higher momenta.

3. $\Upsilon(4S) \rightarrow non - B\bar{B}$

In 1990, both CLEO and ARGUS reported[1] evidence for the production of ψ's with momenta above the kinematic limit for $B \rightarrow \psi X$. In the continuum-only data sample, however, taken at a center-of-mass energy $\sim$ 50MeV below the $\Upsilon(4S)$ resonance, little evidence of a ψ signal could be found. These observations were interpreted as a signal for the unexpected decay $\Upsilon(4S) \rightarrow \psi X$. With the new CLEO II data, representing twice the integrated luminosity of the CLEO I sample, the ψ signal is now clearly seen in the continuum and the entire set of high momentum ψ's may be accounted for by continuum production only.

The $B \rightarrow \psi X$ branching ratio is relatively large ($\sim$ 1.1%) and therefore B decay is a copious source of ψ's at momenta below the kinematic limit of 1.94 GeV. In selecting ψ candidates, we use a cut at 2.0 GeV, and for comparison with continuum data, express this in terms of $x = p/E_{beam} \leq 0.38$. A clean signal is obtained by reconstructing the ψ in its leptonic decay modes, $\psi \rightarrow e^+e^-$ and $\psi \rightarrow \mu^+\mu^-$, as shown in figure 5 for ψ's within the B kinematic range. The data shown are for $491pb^{-1}$ of $\Upsilon(4S)$ running. The net signal after background subtraction is 256 ± 18 events in the dimuon channel, 196 ± 16 in the dielectron channel.

Dilepton spectra for dileptons with $x \geq 0.38$ are shown in figures 6 and 7 for the CLEO I data and the CLEO II data, respectively. With the signal region defined to lie within 30MeV of the ψ mass, the events are tallied and displayed in table I below. Combining the two data samples for maximum statistical power, we find that on the 4S resonance, the ψ yield is $17 + 19 = 36 \pm 6$ events, with a background of $13.6 + 4.3 = 17.9 \pm 1.3$, for a net signal of 18.1 ± 6.1 events. Below the 4S resonance, the continuum sample yields $10 + 2 = 12 \pm 3.5$ events on a background of $2.9 + 0.7 = 3.6 \pm 1.9$ events, for a net yield (after including a scale factor of 2.1 to account for the different on-resonance and off-resonance luminosities and continuum cross sections) of 17.6 ± 7.4 events. The on-resonance ψ events are thus completely consistent with production from the continuum.

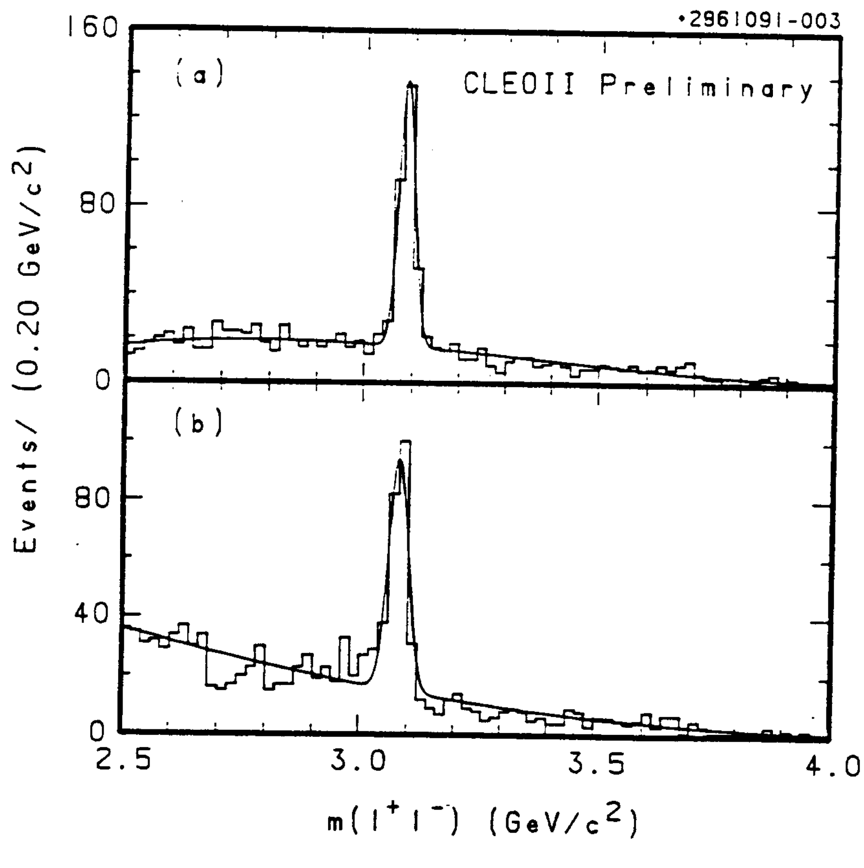

5. Dilepton mass spectra for lepton pairs with total momentum below 1.94 GeV. Upper figure: dimuons; lower figure: dielectrons.

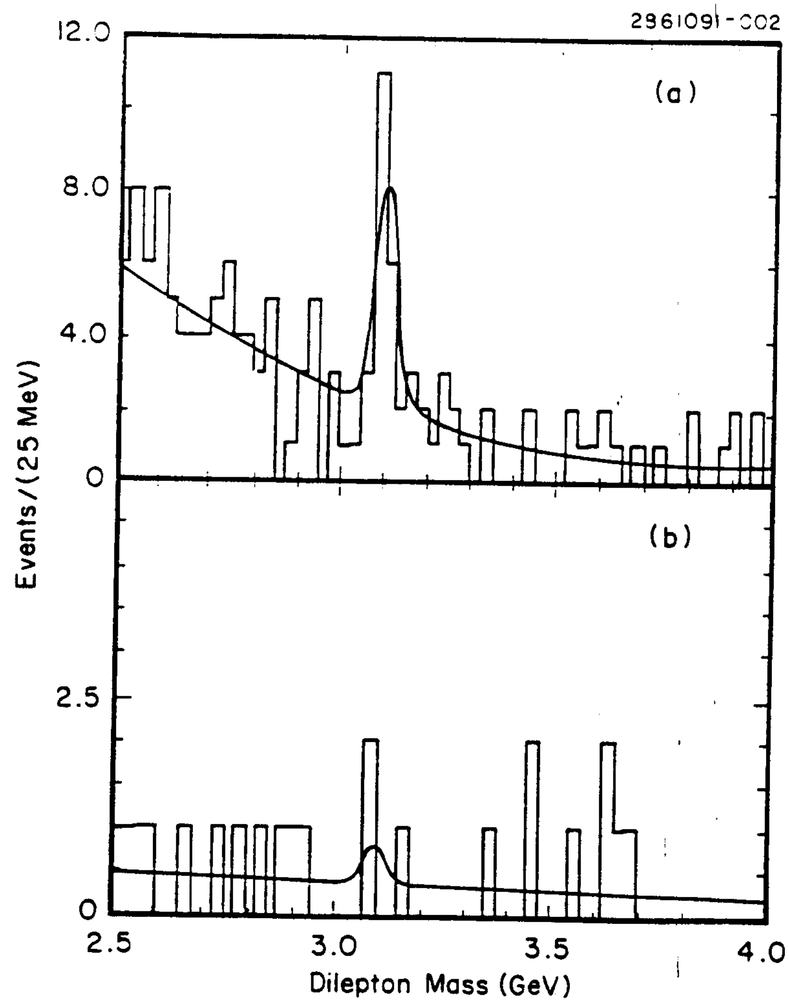

6. Dilepton mass spectra from the CLEO I (1987) data. (a) on the $\Upsilon(4S)$ resonance; and (b) below the resonance (continuum only).

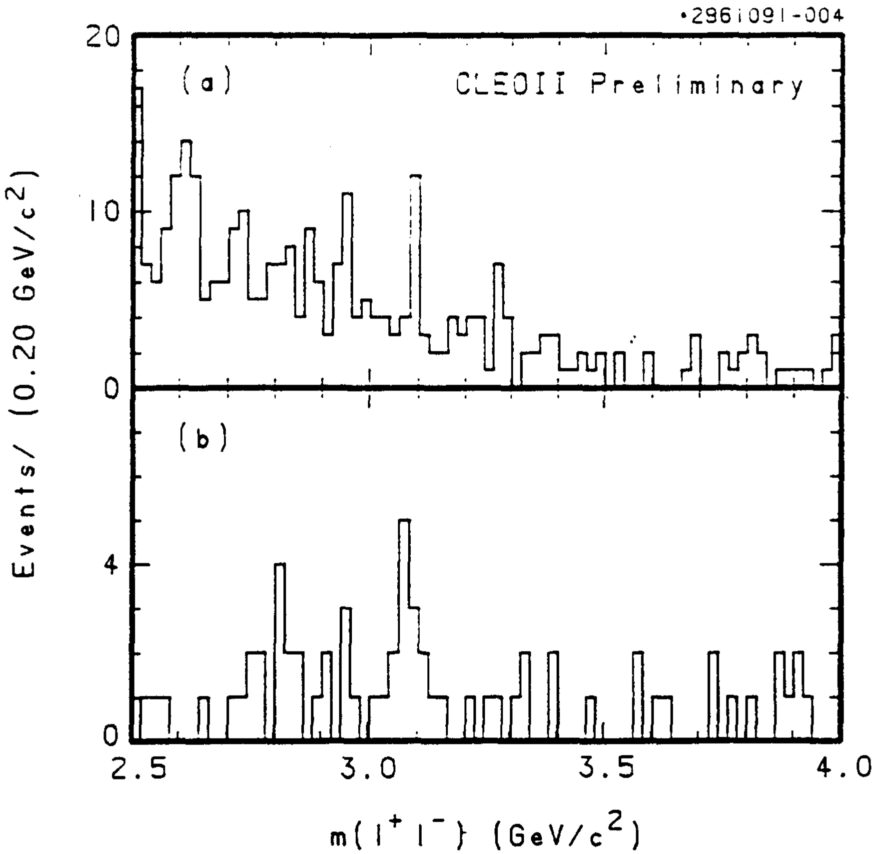

7. Dilepton mass spectra from the CLEO II (1990) data. (a) on the $\Upsilon(4S)$ resonance; and (b) below the resonance (continuum only).

Table I. Yields of High Momentum ψ's.

Data Sample	Signal Region Events	Estimated Background
CLEO II 1990 on resonance	19	13.6 $\pm$1.2
CLEO II 1990 off resonance	10	2.9 $\pm$ 0.5
CLEO I 1987 on resonance	17	4.3 $\pm$ 0.6
CLEO I 1987 off resonance	2	0.7 $\pm$ 0.2

Various models of ψ production are available.[2] These predict the ratio $R = \sigma(e^+e^- \to \psi X)/\sigma(e^+e^- \to \mu^+\mu^-)$ to lie in the range $0.3 \to 2.0 \times 10^{-3}$ for ψ's of $x \geq 0.38$. We measure $R = (1.0 \pm 0.3 \pm 0.3) \times 10^{-3}$. The CLEO I analysis had set a limit, $R \leq 1.9 \times 10^{-3}$ at 90% confidence, consistent with the new measurements.

4. New Measurements of D^* Branching Ratios

Precise knowledge of the D^* branching ratios is an important tool in the study of B decays, and is also an interesting subject in its own right. With $689 pb^{-1}$ of CLEO II data we have made new measurements of all five D^* branching ratios:

$$D^{*+} \to D^0\pi^+,\ D^+\pi^0,\ D^+\gamma$$

and

$$D^{*0} \to D^0\pi^0,\ D^0\gamma.$$

All these have been measured previously,[3] but the $D^{*+} \to D^+\gamma$ has been somewhat controversial as the MARK III measurement of $(17 \pm 5 \pm 5)\%$ is at odds with the theoretical expectations[4] of $\sim 3\%$. The decay is a magnetic dipole transition, and poses no theoretical problems; to explain a large value one must invoke an anomalously large charm quark magnetic moment. With the new CLEO II measurements the large discrepancy between theory and experiment is gone.

The D^0 is reconstructed in its $K^-\pi^+$ mode, and the D^+ in its $K^-\pi^+\pi^+$ mode. Charge conjugate states implied, as usual. D candidates are required to lie within 2σ of the D mass. Time-of-flight measurements and dE/dx determinations are used to establish particle identification of all charged tracks. Photons are observed in the barrel calorimeter, ($|\cos\theta| \leq 0.71$) and are required to exceed 30 MeV as the signal/noise is poor below this level. The π^0 is reconstructed from photon pairs and required to have a mass within 2σ of the π^0 mass; in addition, the decay angle, α, of the photon axis in the rest frame of the π^0, as measured with respect to the π^0 direction, must satisfy $|\cos\alpha| \leq 0.8$ to reduce combinatoric backgrounds. D^* candidates are required to have momentum greater than 2.5GeV, and signal is then determined by a fit to the distribution of $\delta = M_{D^*} - M_D - Q$, where we use the value[8] $Q = 0.1455$ GeV.

Figures 8 to 12 show the δ distributions for the five D^* decay modes. The yields in each of the five modes, together with pertinent mass resolutions and efficiencies are given in table II.

Table II. Raw Data for D^* Decays

Mode	Events	Mass Resolution Measured (MeV)	Mass Resolution Monte Carlo (MeV)	Efficiency
$D^0 \to K^-\pi^+$	10170 ± 197	11.0±0.3	9.5	0.580
$D^+ \to K^-\pi^+\pi^+$	7869±242	10.2±0.3	9.0	0.500
$D^{*0} \to D^0\gamma$	557±71±40	5.6±0.4	5.2	0.157
$D^{*0} \to D^0\pi^0$	724±56±26	1.10±0.05	1.16	0.154
$D^{*+} \to D^+\gamma$	79±59±40		5.2	0.135
$D^{*+} \to D^+\pi^0$	629±37±25	0.95±0.07	1.17	0.133
$D^{*+} \to D^0\pi^+$	2265±61±47	0.80±0.02	0.75	0.47

The branching ratios are extracted by constraining the sum of the three D^{*+} branching ratios to be 1, and similarly for the two D^{*0} branching ratios. The systematic errors that would arise from uncertain D^0 branching ratios are explicitly

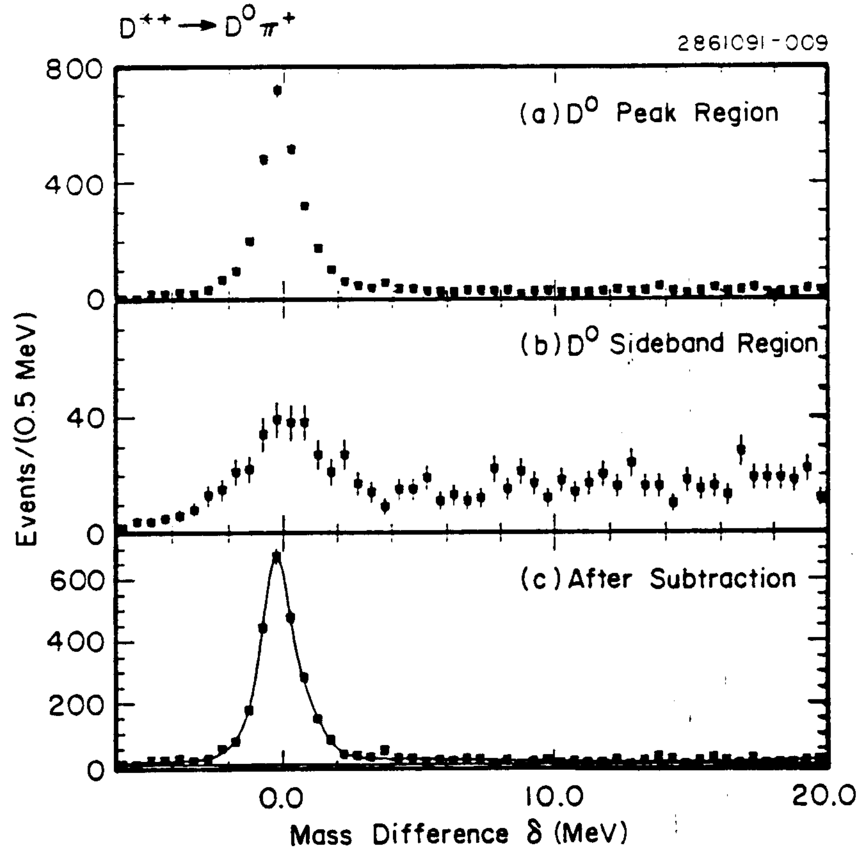

8. Distribution of $M_{D^*} - M_D - Q = \delta$ for $D^{*+} \to D^0\pi^+$

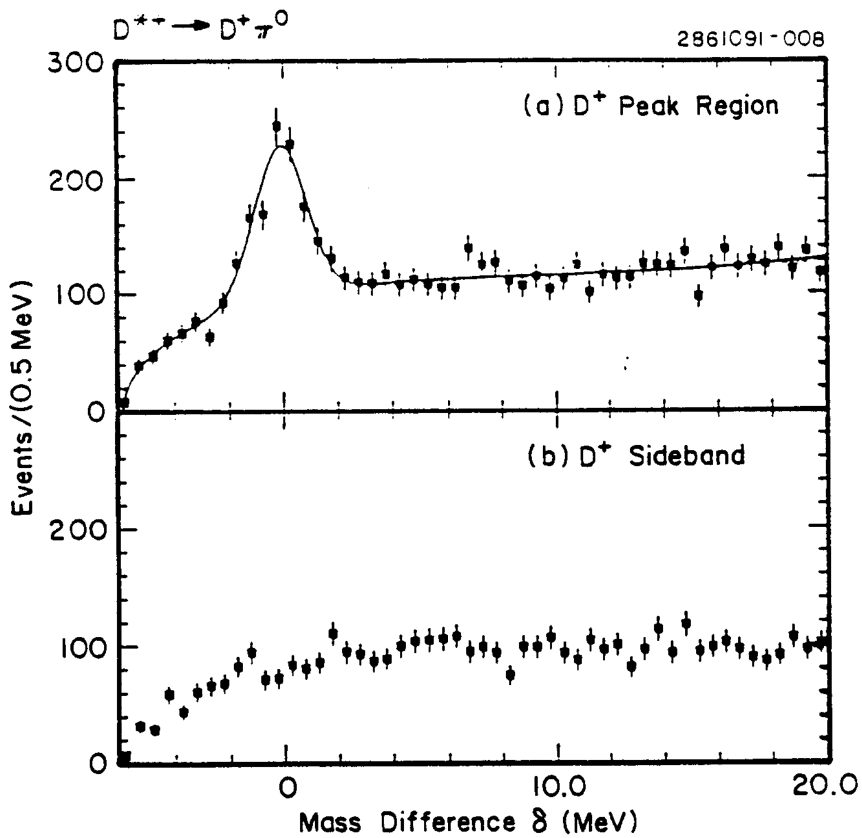

9. Distribution of $M_{D^*} - M_D - Q = \delta$ for $D^{*+} \to D^+\pi^0$

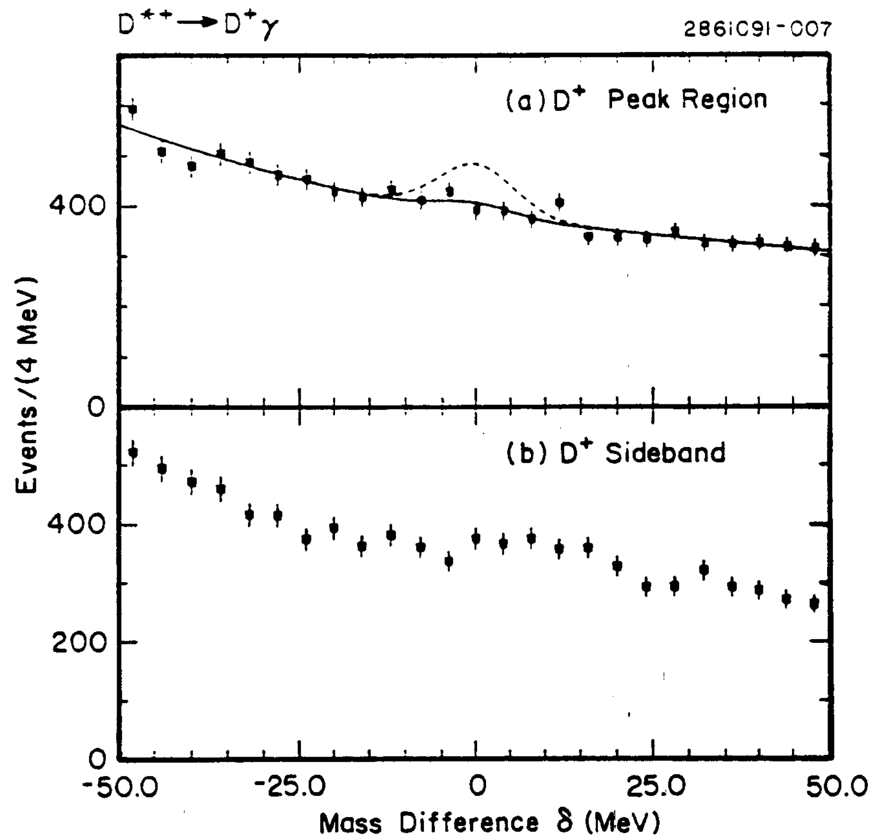

10. Distribution of $M_{D^*} - M_D - Q = \delta$ for $D^{*+} \to D^+\gamma$

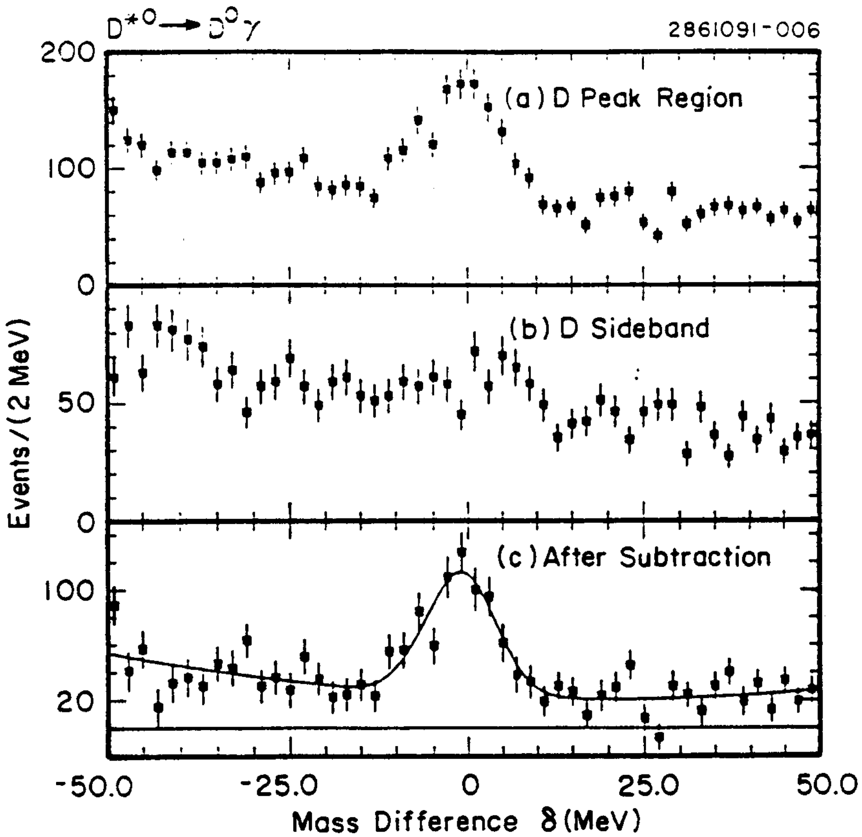

11. Distribution of $M_{D^*} - M_D - Q = \delta$ for $D^{*0} \to D^0\gamma$

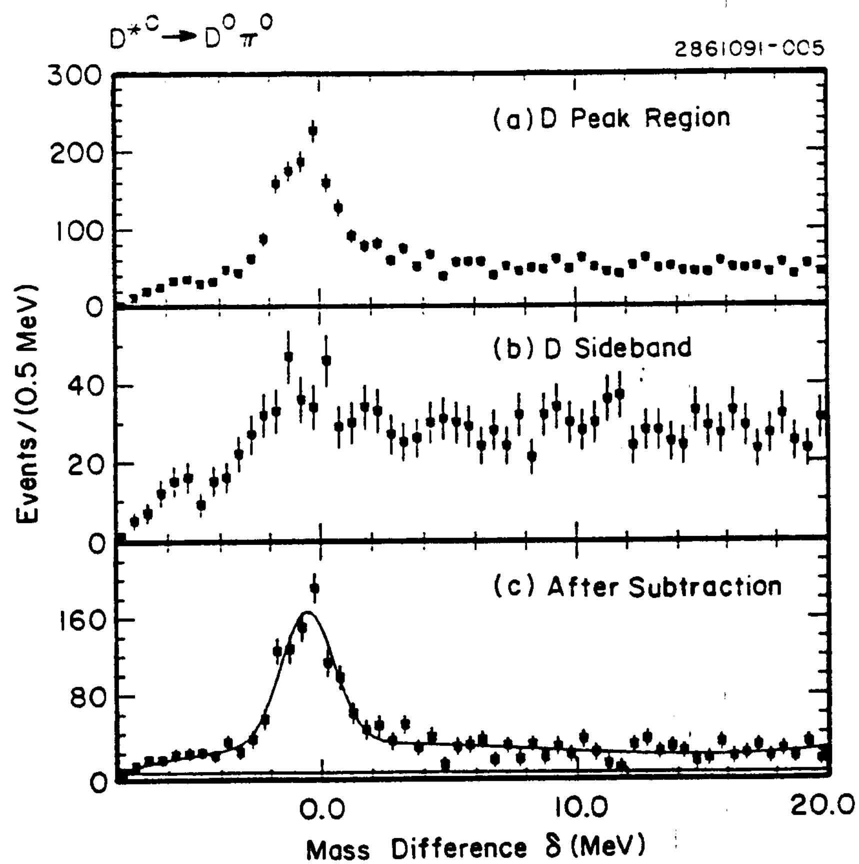

12. Distribution of $M_{D^*} - M_D - Q = \delta$ for $D^{*0} \to D^0\pi^0$

cancelled out by using the ratio

$$R_\gamma^0 = \frac{B(D^{*0} \to D^0\gamma)}{B(D^{*0} \to D^0\pi^0)} = \frac{n(D^0\gamma)}{n(D^0\pi^0)}\frac{\epsilon_{\pi^0}}{\epsilon_\gamma}.$$

Monte Carlo is used to determine the ratio of the efficiencies $\frac{\epsilon_{\pi^0}}{\epsilon_\gamma} = 0.98 \pm 0.15$ after all cuts. This yields a measurement

$$R_\gamma^0 = 0.75 \pm 0.11 \pm 0.13.$$

In conjunction with the sum rule,

$$B(D^{*0} \to D^0\gamma) + B(D^{*0} \to D^0\pi^0) = 1$$

this result gives us the D^{*0} branching ratios, given in table III below. The D^{*+} is similiar, but as there are three decay modes, we measure two ratios,

$$R_\gamma^+ = \frac{B(D^{*+} \to D^+\gamma)}{B(D^{*+} \to D^+\pi^0)} = \frac{n(D^+\gamma)}{n(D^+\pi^0)}\frac{\epsilon_{\pi^0}}{\epsilon_\gamma}$$

and

$$R_\pi^+ = \frac{B(D^{*+} \to D^0\pi^+)}{B(D^{*+} \to D^+\pi^0)} = \frac{n(D^0\pi^+)}{n(D^+\pi^0)}\frac{\epsilon_{D^+\pi^0}}{\epsilon_{D^0\pi^+}}\frac{B(D^+)}{B(D^0)}.$$

In the latter case the D branching ratios do not cancel, and propagate through to non-negligible systematic errors in the final result. D^{*+} branching ratios calculated in this way are given in Table III under the column labelled "Experimental Ratios." One may circumvent this problem, however, by noting that the $D^{*+} \to D^0\pi^+$ and $D^{*+} \to D^+\pi^0$ branching ratios are related through an isospin factor (2) and a momentum dependence (p^3) of the p-wave transition:

$$R_\pi^+ = \frac{B(D^{*+} \to D^0\pi^+)}{B(D^{*+} \to D^+\pi^0)} = 2 \times \left(\frac{p_{+0}}{p_{++}}\right)^3 = 2.19 \pm 0.17.$$

With this value of R_π^+ one obtains the branching ratios given in table III under the column labelled "With Isospin Constraint."

Table III. D^* Branching Ratios

Decay Mode	Experimental Ratios %	With Isospin Constraint %	PDG Values %
$B(D^{*0} \to D^0\gamma)$	43.0±3.7±4.2		45±6
$B(D^{*0} \to D^0\pi^0)$	57.0±3.7±4.2		55±6
$B(D^{*+} \to D^+\gamma)$	3.8±2.8±2.0±0.4	3.7±2.7±1.9	18±4
$B(D^{*+} \to D^+\pi^0)$	30.9±1.6±4.4±3.0±	30.2±0.8±1.6	27.2±2.5
$B(D^{*+} \to D^0\pi^+)$	65.3±2.4±5.1±3.3	66.1±1.8±2.2	55±4

The branching ratio $B(D^{*+} \to D^+\gamma)$ is seen in table III to be consistent with theoretical expectation, and inconsistent with previous results. We may also express this as a 90% confidence limit, $B(D^{*+} \to D^+\gamma) \leq 8.0\%$.

5. New Measurements of D^0 Branching Ratios

The CLEO II cesium-iodide calorimeter has made possible a number of new or improved branching ratio measurements, including the D^0 branching ratios listed below:

$$D^0 \to \pi^0\pi^0, \quad \bar{K}^0\pi^0, \quad \bar{K}^0\eta, \quad \bar{K}^0\eta'.$$

The measurement of $D^0 \to \pi^0\pi^0$ has not previously been measured, and brings to completion the set of all measured decays of D^0 to K's and π's. The remaining determinations are not new, but are considerably improved.

The two-π^0 mass spectrum from $655 pb^{-1}$ of CLEO II data is shown in figure 13. The D^0 candidates are tagged with a D^{*+} or D^{*0}, and the cosine of the decay angle of the π^0 in the D^0 rest frame is required to lie in the range $-0.7 \to 0.7$. Table IV below shows efficiencies and yields for both $D^0 \to \pi^0\pi^0$ and the normalizing mode, $D^0 \to K^-\pi^+$, with both D^* tags. Using $B(D^0 \to K^-\pi^+) = (3.71 \pm 0.25)\%$

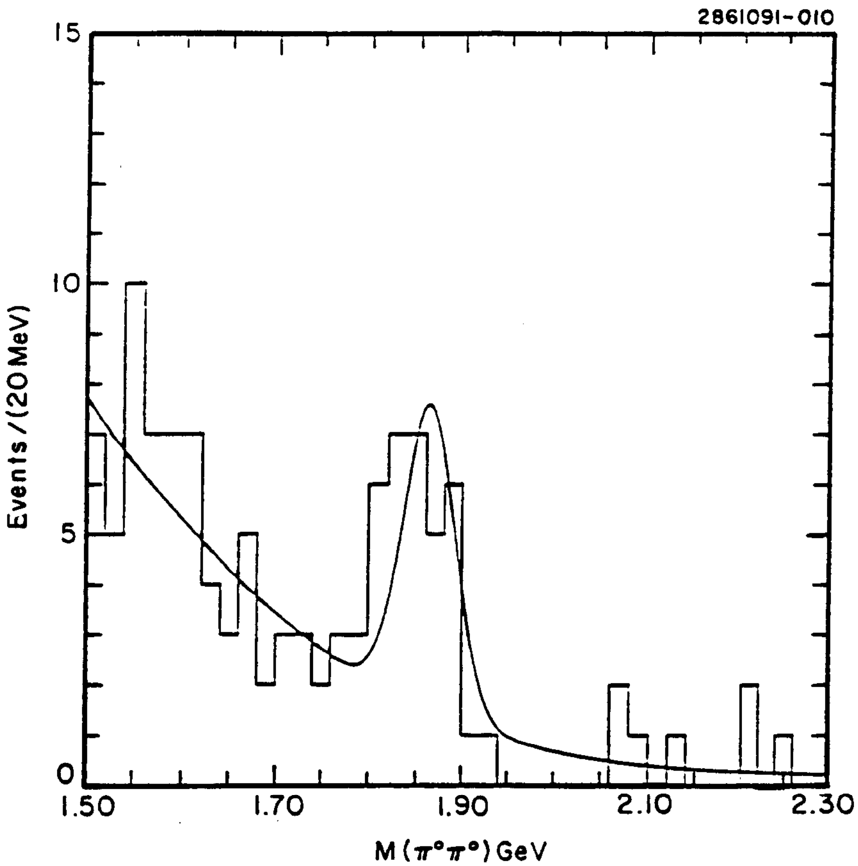

13. $\pi^0\pi^0$ mass spectrum

from the PDB,[5] we obtain

$$B(D^0 \to \pi^0\pi^0) = (0.09 \pm 0.02 \pm 0.02)\%.$$

From an earlier CLEO measurement[6] of $D^0 \to \pi^+\pi^-$ we obtain

$$\frac{B(D^0 \to \pi^0\pi^0)}{B(D^0 \to \pi^-\pi^+)} = 0.50 \pm 0.19.$$

Table IV: Yields and Efficiencies for D^0 Decays

	$D^{*+} \to \pi^+ D^0$		$D^{*0} \to \pi^0 D^0$	
	$D^0 \to \pi^0\pi^0$	$D^0 \to K^-\pi^+$	$D^0 \to \pi^0\pi^0$	$D^0 \to K^-\pi^+$
Efficiency	0.10±0.02	0.40±0.04	0.05±0.01	0.16±0.02
# Events	14.0±4.7	2676±55	11.0±4.7	1139±40

In addition to the π^0 modes, the new calorimeter has made possible the study of decay modes involving both the η and the η'. The η is detected in both its 2γ mode ($B(\eta \to \gamma\gamma) = 39\%$) and its 3π mode ($B(\eta \to \pi^+\pi^-\pi^0) = 24\%$). Mass spectra for these channels are illustrated in figure 14. The lower curve in 14a is obtained by excluding any photon candidate that can pair with some other photon in the event to make a valid π^0 candidate of momentum greater than 0.8 GeV. The η mass peak has a width of 14MeV in the 2γ mode, a width of 6MeV in the 3π mode.

The η' is reconstructed in its $\eta\pi\pi$ mode ($B(\eta' \to \eta\pi^+\pi^-) = 44\%$) and its $\rho^0\gamma$ ($B(\eta' \to \rho^0\gamma) = 30\%$) decay modes, shown in figure 15. The η' mass resolutions are 5MeV and 11MeV for these two modes. In the latter mode the ρ is defined by $\pi^+\pi^-$ pair with invariant mass between 500 and 850 MeV. Since, moreover, the η' is spinless, the ρ must be polarized along the axis defined by the photon direction in the ρ rest frame. The $\pi^+\pi^-$ direction is therefore distributed as $\sin^2\theta_\pi$ where θ_π is the angle between photon and π^+ directions in this frame. A cut requiring $|\cos\theta_\pi| \leq 0.8$ is imposed to enhance signal/background.

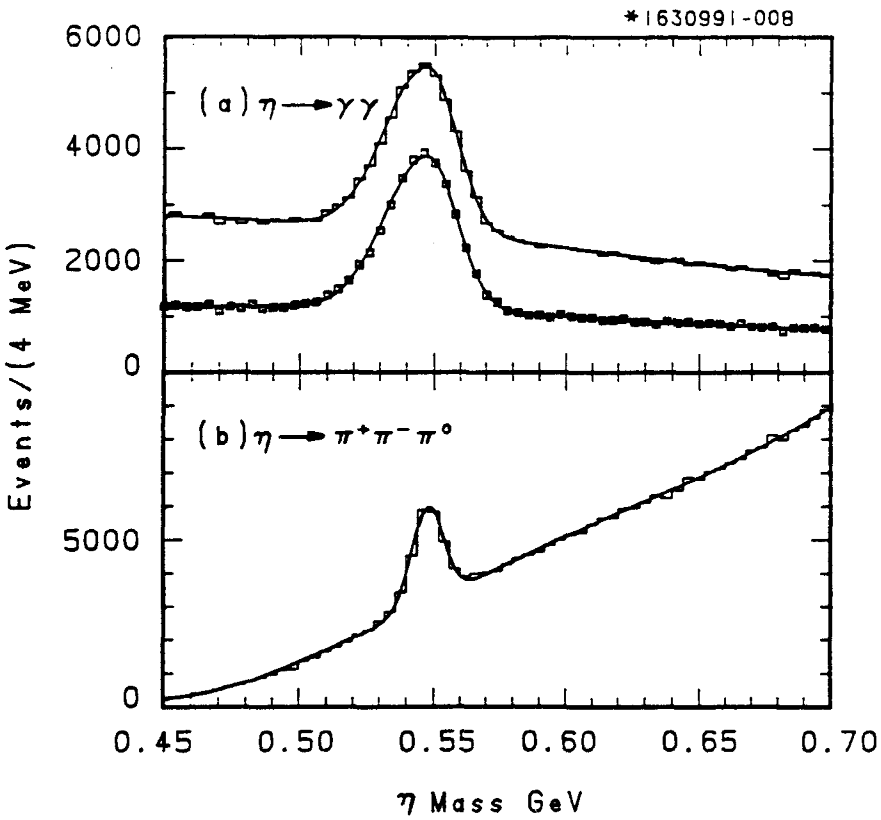

14. η mass spectra for (a) the 2γ and (b) the 3π modes.

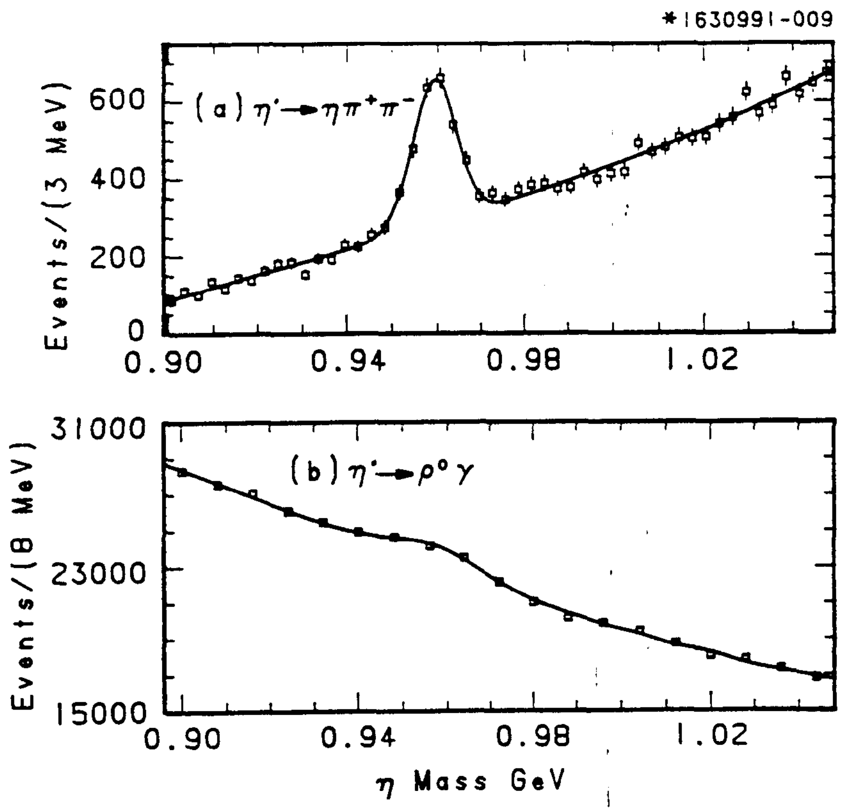

15. η'mass spectrum for (a) the $\eta\pi^+\pi^-$ and (b) the $\rho^0\gamma$ decay modes.

The decays $D^0 \to \bar{K}^0\eta$ and $D^0 \to \bar{K}^0\eta'$ are searched for using the 2γ decay of the η and the $\rho\gamma$ decay of the η'. In the case of $D^0 \to \bar{K}^0\eta'$, a D^* tag is required. Branching ratios are extracted by normalizing to the $D^0 \to K_S\pi^+\pi^-$ channel so that the K_S reconstruction efficiency cancels out. Table V summarizes the raw yields, efficiencies (not including branching ratios), and mass resolutions in each of these modes. We have also examined the mode $D^0 \to K_S\pi^0$ and these results are included in the table. Tables VI and VII give the final branching ratios obtained, and comparison with available theoretical calculations.

Table V: Yields and Efficiencies for D^0 Decays

Mode	Efficiency	Events	σ_{meas} (MeV)	σ_{MC} (MeV)
$K_S\eta$	0.085± 0.009	76± 14	14.4± 2.8	17.0± 1.3
$K_S\eta'$	0.12± 0.01	32± 6.6	13.1± 2.9	13.8± 1.1
$K_S\pi^0$	0.12± 0.01	634± 36	21.3± 1.2	23.0± 1.6
$K_S\pi^+\pi^-$	0.20± 0.02	2940± 105	11.3± 0.5	10.0± 1.0

Table VI: D^0 Branching Ratios (%)

Mode	CLEO	ARGUS[7]	MARK III[7]
$\pi^0\pi^0$	0.09±0.02±0.02		
$\bar{K}^0\pi^0$	1.99±0.13±0.30	1.7±0.4±0.3	1.8±0.2±0.2
$\bar{K}^0\eta$	0.85±0.15±0.16	1.4±0.5±0.3	1.6±0.6±0.4
$\bar{K}^0\eta'$	2.5±0.5±0.6	1.9±0.4±0.3	3.3±0.8±1.0[8]

Table VII: Predictions of D^0 Branching Ratios (%)

Mode	BSW[9]	BS[10]	Kamal[11]	Rosen[12]
$\pi^0\pi^0$	0.034	0.15	0.23±0.03[a] 0.010±0.014[b]	
$\bar{K}^0\pi^0$	0.8 2.1[c]	1.5		
$\bar{K}^0\eta$	0.31	0.4		0.06-0.25
$\bar{K}^0\eta'$	0.12	1.2		1.7-6.5

(a) without final state interactions

(b) with inelastic final state interactions

(c) with elastic final state interactions

6. New Measurements of D_s Branching Ratios

With the new calorimeter and the clean η and η' signals now available, CLEO has been able to measure with ~20% precision the long-controversial decays of the D_s to states involving the η and η', namely $D_s^+ \to \eta\pi^+$ and $D_s^+ \to \eta'\pi^+$. In addition, measurements of the hitherto inaccessible decays $D_s^+ \to \eta\rho^+$ and $D_s^+ \to \eta'\rho^+$ have become possible and will be reported here.

With the η reconstructed as described earlier, the $\eta\pi^+$ mass distributions are shown in figure 16. The background shape includes a guassian for $D^+ \to \eta\pi^+$ as well as a small contribution from incompletely reconstructed $D_s \to \eta\rho^+$. In the latter case, the shape is taken from Monte Carlo, and the normalization from the measurement to be described subsequently. Yields and efficiencies for this mode and all other modes to be discussed are summarized in table VIII below. Branching ratios expressed in terms of $D_s \to \phi\pi$ are also be given in that table.

Figure 17 shows the invariant mass distributions for $\eta'\pi^+$ combinations. The background shape includes, as in the previous case, a gaussian for the D^+ and

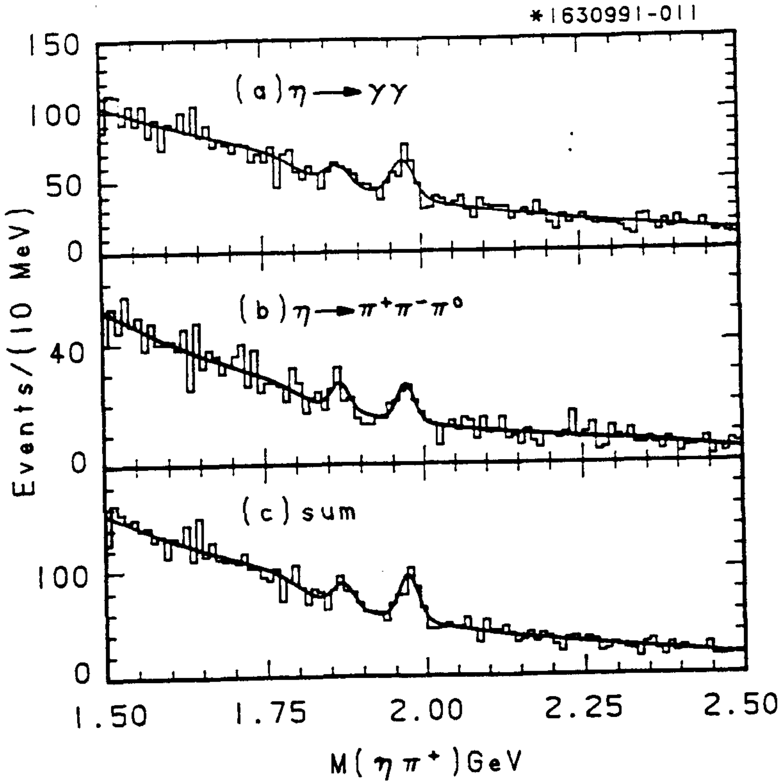

16. $\eta\pi^+$ mass distributions, for the two decay modes of the η and the sum, as labelled.

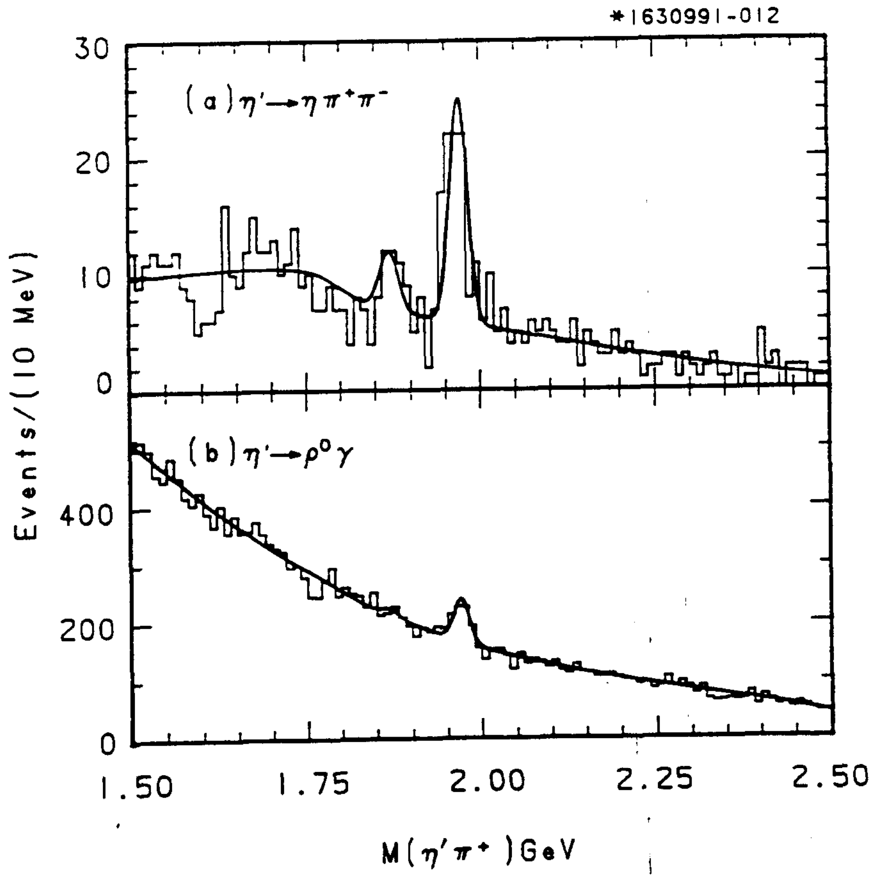

17. Mass distributions of $\eta'\pi^+$ for two η' decays modes, as labelled.

a Monte Carlo-determined shape for incompletely reconstructed decay $D_s \to \eta' \rho$. Yields, efficiencies, and results are in table VIII.

The decays $D_s \to \eta\rho$ and $D_s \to \eta'\rho$ pose additional challenges in the identification of the ρ. Figure 18 shows the invariant mass distribution of $\eta\pi^+\pi^0$ with a peak at the D_s. In this case the $\pi^+\pi^0$ candidates are required to lie within 170MeV of the ρ mass, and helicity angle cut, $|\cos\theta_\pi| \geq 0.45$ is imposed. The angle θ_π is the angle between the π^+ and the direction of the ρ, in the ρ rest frame. Since both the D_s and the η are spinless, the ρ must have zero helicity, and hence the angular distribution of the pions will be $\cos^2\theta_\pi$, and signal/background is enhanced by the above cut. The features of the $\pi^+\pi^0$ system are illustrated in figure 19a where the invariant mass of the dipion system is plotted for events in the D_s peak, which show peaking at the ρ mass, as well as from the sidebands, which do not. In figure 19b the helicity angular distribution is consistent with $\cos^2\theta_\pi$ as expected for genuine ρ decay. The distribution of figure 19b puts a limit of 20% on nonresonant $\pi^+\pi^0$ combinations; a more stringent limit may be derived by considering also the mass distribution of the dipion system, resulting in an upper limit of 7% nonresonant contribution, at 90% confidence.

The analysis of $D_s \to \eta'\rho$ is similiar. In this case only the decay mode $\eta' \to \eta\pi^+\pi^-$ is used, to avoid backgrounds that arise when $\eta' \to \rho^0\gamma$ is used. Figure 20 illustrates the invariant mass distribution under the requirement that the dipion system lie within 170MeV of the the ρ mass. Solid squares in the figure are for the case where the dipion mass is below 500 MeV. (Note that because the maximum energy available to the dipion system is only about 1GeV, there is no upper sideband available.) Figure 21a illustrates the mass distribution of the dipion system, showing a peak at the ρ mass only for those events under the D_s peak. Figure 21b shows the corresponding helicity angle distribution which is fit to $\cos^2\theta_\pi$. As done for the $\eta\rho$ case, an upper limit of 8% is set for non-resonant $\pi^+\pi^0$ contribution.

All measurements of these D_s decays are summarized in table VIII. The table

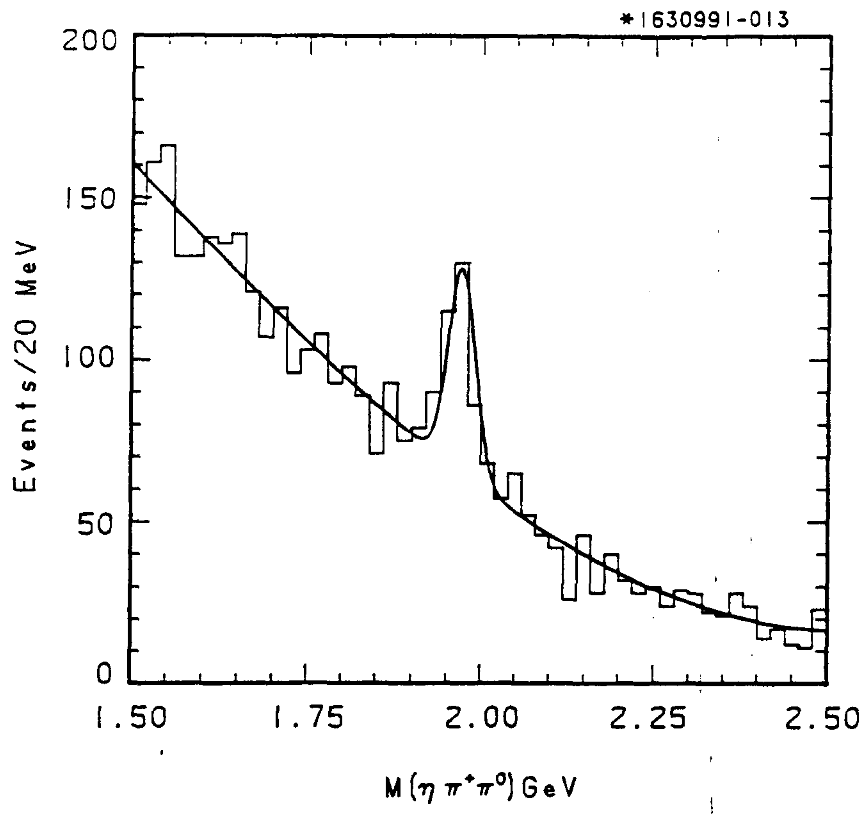

18. Invariant mass distribution for $\eta\pi^+\pi^0$. Only $\eta \to \gamma\gamma$ is used in this plot. Additional requirements are discussed in the text.

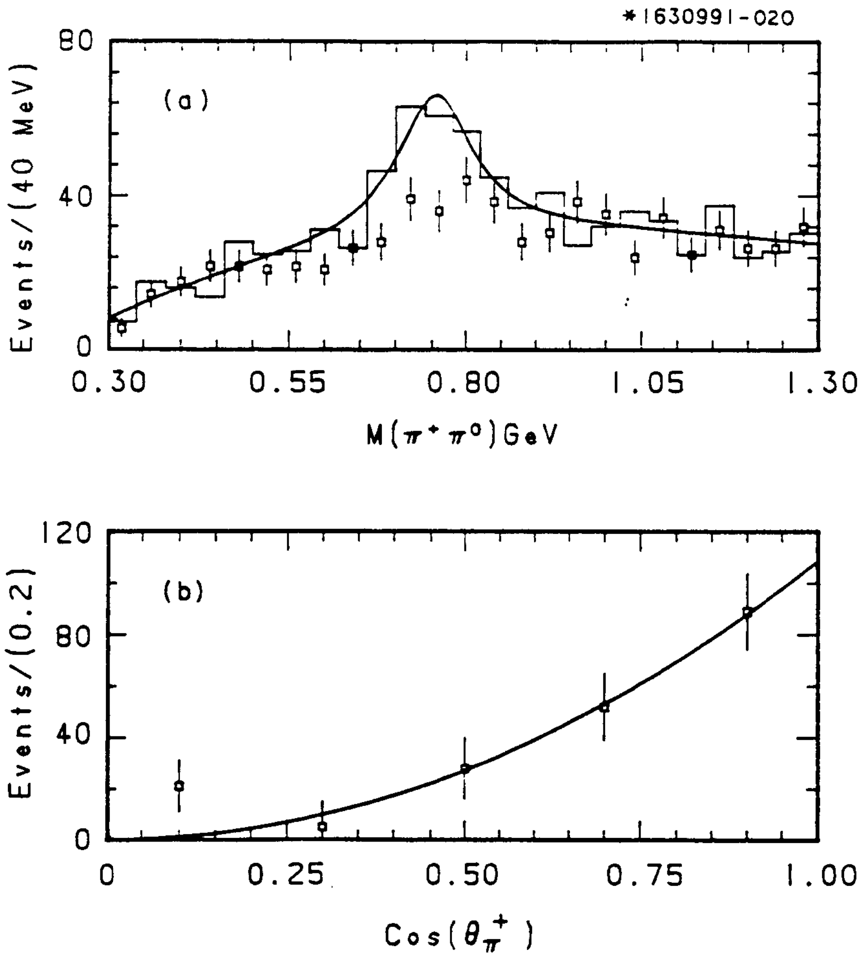

19. (a) $\pi^+\pi^0$ mass distribution for events in the D_s peak (histogram) of figure 18 and in the sidebands (points). (b) distribution of events in the D_s peak as a function of the helicity angle, $\cos\theta_\pi$. The $\pi^+\pi^0$ combination must lie within 170 MeV of the ρ mass.

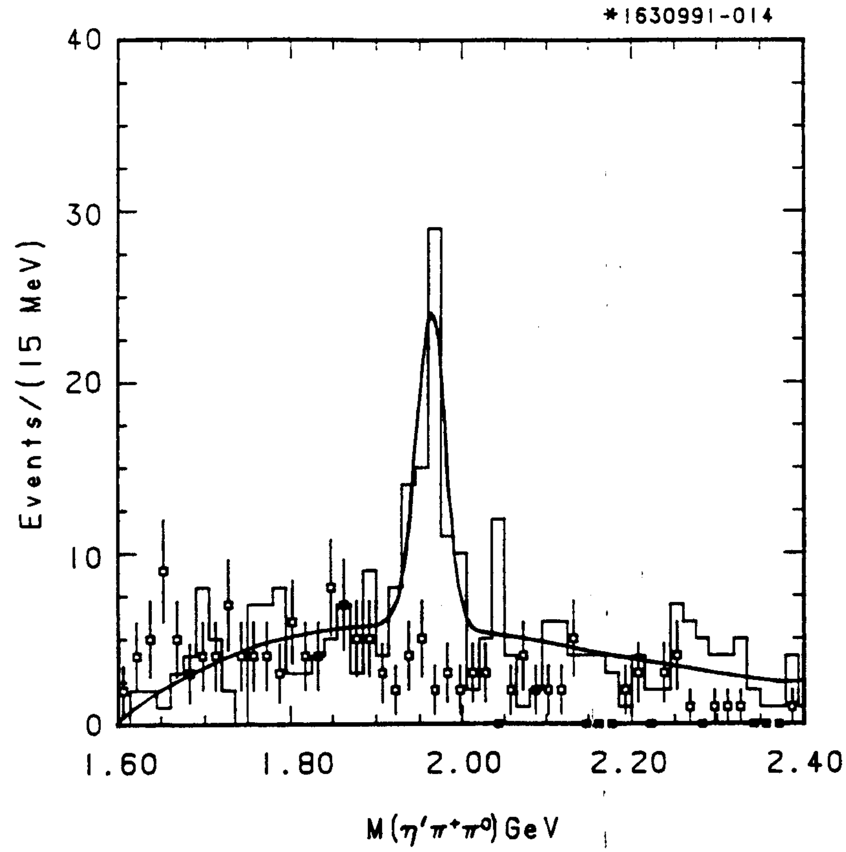

20. Invariant mass distribution for $\eta'\pi^+\pi^0$ ($\eta' \to \eta\pi^+\pi^-$, $\eta \to \gamma\gamma$).

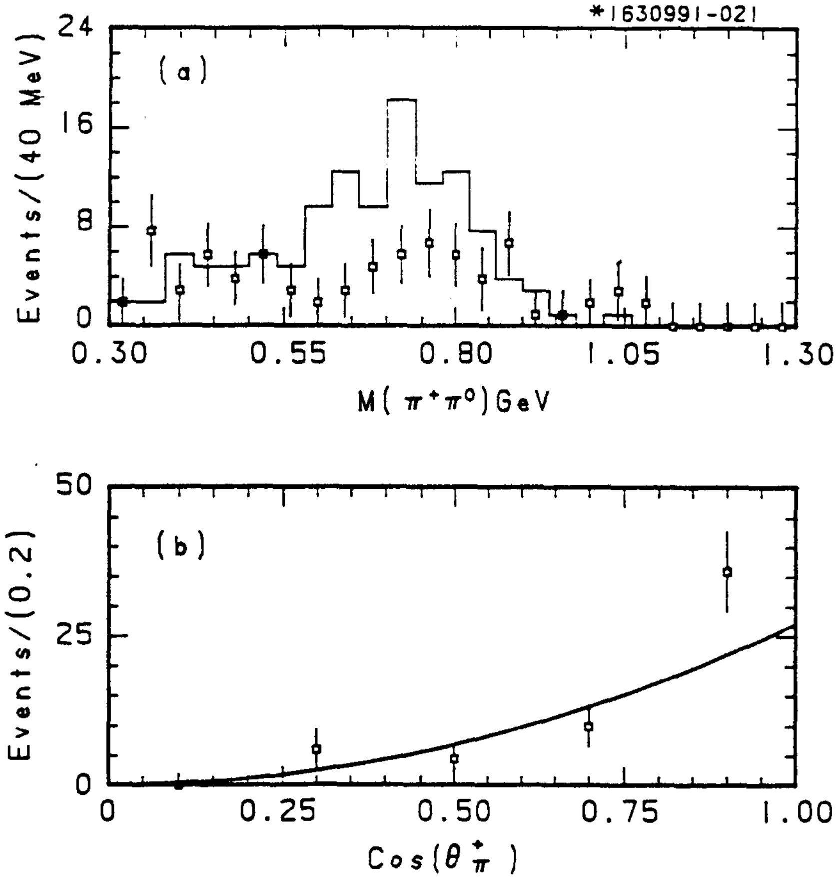

21. (a) Invariant mass distribution for $\pi^+\pi^0$ pairs from events under the D_s peak (histogram) and from the D_s sidebands (solid points). (b) Helicity angle distribution for the ρ candidates.

breaks out the many decay subchannels and gives the branching ratio (relative to $D_s \to \phi\pi$) for each subchannel. The column labelled $\epsilon \times B$ is the acceptance times branching ratios for the D_s daughters. Table IX provides the branching ratio for each primary D_s decay channel, a weighted average over the subchannels, and also gives current theoretical predictions.

Table VIII. D_s Branching Ratios

Mode	$s\bar{s}$ Decay	Events	MC Width (MeV)	$\epsilon \times B$ (%)	B/B($\phi\pi$)
$\phi\pi$	$\phi \to K^+K^-$	453±28	8.7	17.0	1
$\eta\pi$	$\eta \to \gamma\gamma$	123±24	19	8.17	0.56±0.11± 0.07
	$\eta \to \pi^+\pi^-\pi^0$	42±12	14	3.14	0.49±0.15±0.07
$\eta'\pi$	$\eta' \to \eta\pi^+\pi^{-a}$	59±11	13	2.05	1.10±0.21±0.12
	$\eta' \to \rho^0\gamma$	200±34	11	5.40	1.38±0.25± 0.20
	$\eta' \to \eta\pi^+\pi^{-b}$	22±7	12	0.75	1.12±0.36± 0.15
$\eta\rho^+$	$\eta \to \gamma\gamma$	158±22	20	2.02	2.93±0.45 ±0.39
	$\eta \to \pi^+\pi^-\pi^0$	59±15	20	0.82	2.70±0.68±0.38
$\eta'\rho^+$	$\eta' \to \eta\pi^+\pi^{-a}$	53±10	20	0.56	3.55±0.71±0.53
	$\eta' \to \eta\pi^+\pi^{-b}$	15±6	20	0.18	3.10±1.24 ±0.45
$\phi\rho^+$	$\phi \to K^+K^-$	253±32	13	5.10	1.86±0.26±0.29

a. $\eta \to \gamma\gamma$

b. $\eta \to \pi^+\pi^-\pi^0$

Table IX. Relative Branching Ratios and Theoretical Predictions

Mode	$B/B(\phi\pi)$				
	This Experiment	BSW[9]	BSW'[13]	KSS[13]	BS[10]
$\phi\pi^+$	1	1	1	1	1
$\eta\pi^+$	$0.54\pm0.09\pm0.06$	1.04	0.75	1.35	1.13
$\eta'\pi^+$	$1.20\pm0.15\pm0.11$	0.61	0.78	1.47	0.10
$\eta\rho^+$	$2.86\pm0.38^{+0.36}_{-0.38}$	1.96			2.33
$\eta'\rho^+$	$3.44\pm0.62^{+0.44}_{-0.46}$	0.56			
$\phi\rho^+$	$1.86\pm0.26^{+0.29}_{-0.40}$	6.30			

7. Conclusions

A wide range of charm decay modes have been studied, with special attention paid to modes involving neutrals. In addition, new results on high momentum ψ production at 10.6 GeV have been presented; The measurements are consistent with continuum origin of the ψ's.

8. Acknowledgements

The work was supported by the National Science Foundation and the Department of Energy. The author gratefully acknowledges the support of the PYI program of the NSF.

REFERENCES

1. J.P. Alexander *et al.*, (CLEO Collaboration), Phys. Rev. Lett. **64**,2226 (1990);
   M. Danilov, in Z^0 *Physics, proceedings of the XXVth Rencontre de Moriond*, Editions Frontieres, France (1990).
2. H. Fritzsch and J. H. Kühn, Phys. Lett. **B90**, 164 (1980);
   W.-Y. Keung, Phys. Rev. **D23**, 2072 (1981);
   J. H. Kühn and H. Schneider, Z. Phys. **C11**, 263 (1981).
3. J. Adler *et al.*, Phys. Lett. **B208**, 152 (1988).
4. S. Ono, Phys. Rev. Lett. **37**, 655 (1976);
   E. Eichten *et al.*, Phys. Rev. **D21**, 227 (1980);
   W. Wilcox, O.V. Maxwell, K.A. Milton, Phys. Rev. **D31**, 1081 (1985);
   R.L. Thews, A.N. Kamal, Phys. Rev. **D32**, 810 (1985);
   L. Brekke, J. Rosner, Comm. Nucl. Part. Phys. **18**, 83 (1988);
   G.A. Miller, P. Singer, Phys. Rev. **D37**, 2564 (1988);
   E. Angelos, G.P.Lepage (private communication).
5. Particle Data Group, J. J. Hernandez *et al.*, Phys. Lett. **B239**, 1 (1990).
6. J.P. Alexander *et al.*, Phys. Rev. Lett. **65**,1184 (1990).
7. ARGUS and MARK III results as summarized by P.E. Karchin in Proceedings of the 1989 International Symposium on Lepton and Photon Interactions at High Energies, ed. Michael Riordan, World Scientific, Singapore, p105, (1990).
8. J.F. Labs, Proceedings of the Twelfth International Conference on Particles and Nuclei, eds. J.L. Matthews, T.W. Donnelly, E.H. Farhi, and L.S. Osborne, North Holland, Amsterdam, p753c (1991).
9. M. Bauer, B. Stech, and M. Wirbel, Z. Phys. **C34**, 103 (1987).
10. B. Yu. Blok and M. A. Shifman, Sov. J. Nucl. Phys. **45**, 522, (1987).

11. A. N. Kamal, presented at IVth Conference on Intersections between Particle and Nuclear Physics, Tucson, Arizona, (1991), Alberta-THY-23-91.

12. S. P. Rosen, Phys. Rev. **D39**,1349 (1989).

13. A.N. Kamal, N. Sinha, and R. Sinha, Phys. Rev. **D38**, 1612 (1988). For the column labelled BSW', BSW[9] is modified by using $\eta - \eta'$ mixing angle to be -19^o instead of -11^o degrees. *cf*. F. J. Gilman and R. Kauffman, Phys. Rev. **D36**, 2761 (1987).